Advances in Imaging Secondary Ion Mass Spectrometry for Biological Samples

Steven G. Boxer,[1] Mary L. Kraft,[2] and Peter K. Weber[3]

[1]Department of Chemistry, Stanford University, Stanford, California 94305; email: sboxer@stanford.edu

[2]Department of Chemical and Biomolecular Engineering, University of Illinois, Urbana-Champaign, Urbana, Illinois 61801; email: mlkraft@illinois.edu

[3]Glenn T. Seaborg Institute, Lawrence Livermore National Laboratory, Livermore, California 94551; email: weber21@llnl.gov

Annu. Rev. Biophys. 2009. 38:53–74

First published online as a Review in Advance on December 16, 2008

The *Annual Review of Biophysics* is online at biophys.annualreviews.org

This article's doi: 10.1146/annurev.biophys.050708.133634

1936-122X/09/0609-0053$20.00

Key Words

membrane organization, chemical composition imaging, NanoSIMS, ToF-SIMS, dynamic SIMS

Abstract

Imaging mass spectrometry combines the power of mass spectrometry to identify complex molecules based on mass with sample imaging. Recent advances in secondary ion mass spectrometry have improved sensitivity and spatial resolution, so that these methods have the potential to bridge between high-resolution structures obtained by X-ray crystallography and cyro-electron microscopy and ultrastructure visualized by conventional light microscopy. Following background information on the method and instrumentation, we address the key issue of sample preparation. Because mass spectrometry is performed in high vacuum, it is essential to preserve the lateral organization of the sample while removing bulk water, and this has been a major barrier for applications to biological systems. Recent applications of imaging mass spectrometry to cell biology, microbial communities, and biosynthetic pathways are summarized briefly, and studies of biological membrane organization are described in greater depth.

Contents

INTRODUCTION

Structural biology has seen huge advances during the past 20 years due to the confluence of efficient methods for protein overexpression and purification, synchrotron X-ray sources, and array detectors. As a result, we now have the three-dimensional structures of many proteins, including membrane proteins and large assemblies such as the ribosome. These structures provide the basic level of organization of biological systems, often at atomic resolution, on the length scale up to roughly 10 nm. The development of new methods for obtaining information on the organization and dynamics of assemblies on a longer length scale, such as the lateral organization of proteins and lipids in a biological membrane, is an important frontier in structural biology. Many types of imaging methods and microscopies seek to fill this need. This review focuses on secondary ion mass spectrometry (SIMS), still in its infancy as applied to biological systems. This approach to biological imaging has the potential to bridge between atomic-level structures and conventional light microscopy by providing direct compositional information at the 50 nm to several micron length scale. Comparisons with other state-of-the-art imaging methods are briefly discussed in the concluding section.

Conventional mass spectrometry has been transformed from a method largely limited to analytical chemistry and geochemistry into an indispensable tool for the characterization of biological molecules and even assemblies. This is the result of revolutionary advances in matrix-assisted laser desorption/ionization (MALDI) (14, 15, 70, 91, 104) and electrospray ionization (48, 114) methods. Both methods deliver large molecules into the gas phase, where they are ionized so that their mass-to-charge ratio can be measured with high precision. Further processing into fragments (tandem mass spectrometry) can provide high-resolution information on molecular level structure, and by clever use of isotopes, even the kinetics of assembly of large complexes can be characterized (105). These once exotic methods have become essential, even routine, analytical tools for all laboratories investigating the structure of biological molecules. The information content of mass spectrometry is extraordinary, leading to unambiguous identification of molecules by their mass. The promise of imaging mass spectrometry is to combine this level of chemical identification with spatial information.

There are two broad classes of imaging mass spectrometry, depending upon the method used to scan the sample and generate an image. The first class is based on MALDI and takes advantage of the laser used to desorb molecules within a matrix from a surface as the laser is scanned across the sample. Typically, pulsed lasers are used to ablate the sample, and the resulting ions or fragments are detected by using a time-of-flight (ToF) mass spectrometer. Because the spot size of the laser is, at best, given by the diffraction limit, lateral resolution less than 1 μm is difficult. Typically, a much larger spot size (>10 microns) is used to produce sufficient secondary ion signal intensity for molecular imaging. This method is routinely applied to organ-scale biomolecule imaging. MALDI imaging of biological samples has recently been reviewed and is not covered further here (14, 71).

SIMS: secondary ion mass spectrometry

MALDI: matrix-assisted laser desorption/ionization

ToF: time of flight

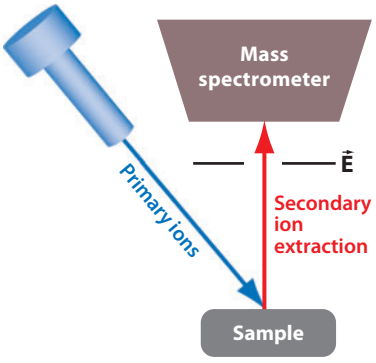

Figure 1

Simplified schematic of a secondary ion mass spectrometry (SIMS) instrument. The common components of all SIMS instruments are a primary ion source, a sample chamber with secondary ion extraction optics, and a mass spectrometer. Mass spectrometers include time-of-flight, magnetic sector, and quadrapoles.

The second class of imaging mass spectrometry, SIMS, is based on the use of an accelerated primary ion beam that bombards the surface and generates secondary ions (**Figure 1**). As described below, lateral resolution better than 100 nm is possible with specialized instruments. SIMS has the potential to image the distributions of specific species within complex biological samples and to measure the amount of each species within a specified region on the sample. Thus, the potential exists for a true analysis of the sample, although many challenges must be resolved before this long-term goal becomes a reality.

There are two fundamentally different approaches to SIMS analysis of biological samples based on the instrument design: ToF-SIMS and dynamic SIMS using a magnetic sector mass spectrometer. For ToF-SIMS, the primary ion beam is pulsed and the resulting secondary ions are detected by a ToF mass spectrometer. This approach allows the full mass spectrum to be monitored during the analysis. The goal of ToF-SIMS is the ejection and detection of molecular species. In contrast, dynamic SIMS is performed with a continuous primary ion beam and a preselected set of ions is detected with a magnetic sector mass spectrometer. Here we use the term "dynamic SIMS" as others have used it. However, ToF-SIMS instruments can be operated in a dynamic mode, meaning that the primary ion beam erodes away the sample surface, exposing fresh sample. This ToF-SIMS approach is typically not used for biological samples because molecular information is lost. A term less used, but potentially more apt, than dynamic SIMS is "magnetic sector SIMS." Typically, in dynamic SIMS, reactive primary ions are used to enhance secondary ion yields. Under continuous ion bombardment, molecular bonds are broken and only monatomic and small molecular ions are produced and detected. In this approach, molecule-specific elemental or isotopic tags are used to locate and quantify molecules of interest.

SIMS is widely used for studying hard materials in materials science, geology, and cosmochemistry. SIMS instruments are commonly found in materials science departments, and they are integrated into semiconductor fabrication for quality control and analysis. By comparison, the application of SIMS to biological sample analysis has been limited, with only a small number of laboratories putting significant effort into biologically related problems. Broadly speaking, the major reasons that SIMS has not historically been more widely adopted for biological sample analysis are (*a*) insufficient sensitivity and spatial resolution, (*b*) challenges of molecular identification, and (*c*) challenges of biological sample preservation for high-vacuum analysis. However, the invention of new ion sources for ToF-SIMS and the development of a high-resolution dynamic SIMS instrument, the NanoSIMS 50 from CAMECA Instruments (16), have raised the potential for SIMS to become a valuable imaging technique in the biosciences. The state-of-the-art of SIMS imaging of biological samples is the subject of this review, with an emphasis on dynamic SIMS; excellent reviews of ToF-SIMS have recently been published (53, 69). We emphasize references from the literature on biological imaging; several reviews on the underlying technology are cited but not discussed in detail.

NanoSIMS: brand name of a high-spatial resolution dynamic SIMS instrument from CAMECA

INSTRUMENTATION

Figure 1 shows a generic scheme for a SIMS instrument. The major components are a primary ion source, a sample chamber, and a secondary ion mass spectrometer. Typically, the primary ion beam column is oriented obliquely to the sample surface, and secondary ions are extracted for analysis by an electrostatic field normal to the surface. This configuration allows the primary ion beam focusing to be independent of the secondary ion beam focusing. CAMECA fundamentally changed this configuration with the introduction of the NanoSIMS 50 by bringing the primary ion beam in normal to the sample surface, coaxial with the secondary ion beam (**Figure 2**). This change enables the primary focusing lens to be brought closer to the sample, thereby reducing focusing aberrations (51, 100). Imaging is performed by scanning the focused primary beam across the sample and digital reconstruction of a map of different masses corresponding to different parent molecules. The best lateral resolution achieved by these instruments is on the order of 50 nm with significant reduction in primary beam current, while 100 nm can be achieved routinely with a beam current of ~2 pA Cs^+. Similar lateral resolution was previously achieved in SIMS with liquid metal sources (63). The NanoSIMS is significant because it achieves this lateral resolution with reactive primary ions, which enhances sensitivity, while maintaining high mass resolving power, which enhances specificity.

ToF-SIMS

For ToF-SIMS, many different primary ion beams have been developed, and this is an active area of research and development. The primary ion beam is accelerated to high energy and focused onto the region of the sample whose composition is being imaged. The interaction of the primary beam with the sample depends on the energy, current, and nature of whatever is accelerated and, in many cases, the environment, or matrix, in which the molecules of interest are embedded (116). A large body of empirical data has been collected (73, 101) and some models are available to guide new developments (32) because each primary ion source involves a substantial engineering and optimization effort. Each primary ion beam offers different advantages for the generation of secondary ions. For biological samples, the emphasis in recent years has been on larger projectiles such as gold clusters as large as several hundred gold atoms (66), Bi_3^+, SF_5^+, or C_{60}^+, because these primary ions open the potential for higher yields of large molecules. Large secondary ion fragments are desirable because biological samples typically contain complex mixtures and larger fragments have greater chemical information than smaller ones do. At the same time, the amounts of each component in the sample area are often low, so high sensitivity is also at a premium. Unfortunately, most of the species ejected from the surface are neutral and therefore not detected by the mass spectrometer. This factor is the primary limitation on detecting and imaging low-abundance molecules. Post-ionization of the neutrals is possible, although further fragmentation of molecules is a primary challenge for this approach (49, 115). A great deal of instrumentation development has been devoted to focusing and rastering the primary ion beam and optimizing secondary ion collection optics, and although beyond the scope of this review, this greatly affects the sensitivity of the measurement (13, 16).

For ToF-SIMS, the primary ion beam is pulsed to enable ToF detection. The secondary ions are accelerated by an electric field to the same kinetic energy; thus the velocity of any individual ion depends on its mass-to-charge ratio (heavier particles move more slowly). By measuring the time for an ion to reach a detector, this mass-to-charge ratio can be obtained with high precision and a wide range of masses can be monitored. The ability to distinguish between adjacent masses is characterized by mass resolving power, which is defined as the nominal mass divided by the difference in mass between the two species ($M/\Delta M$). Because ToF-SIMS ion detection is based on the time of

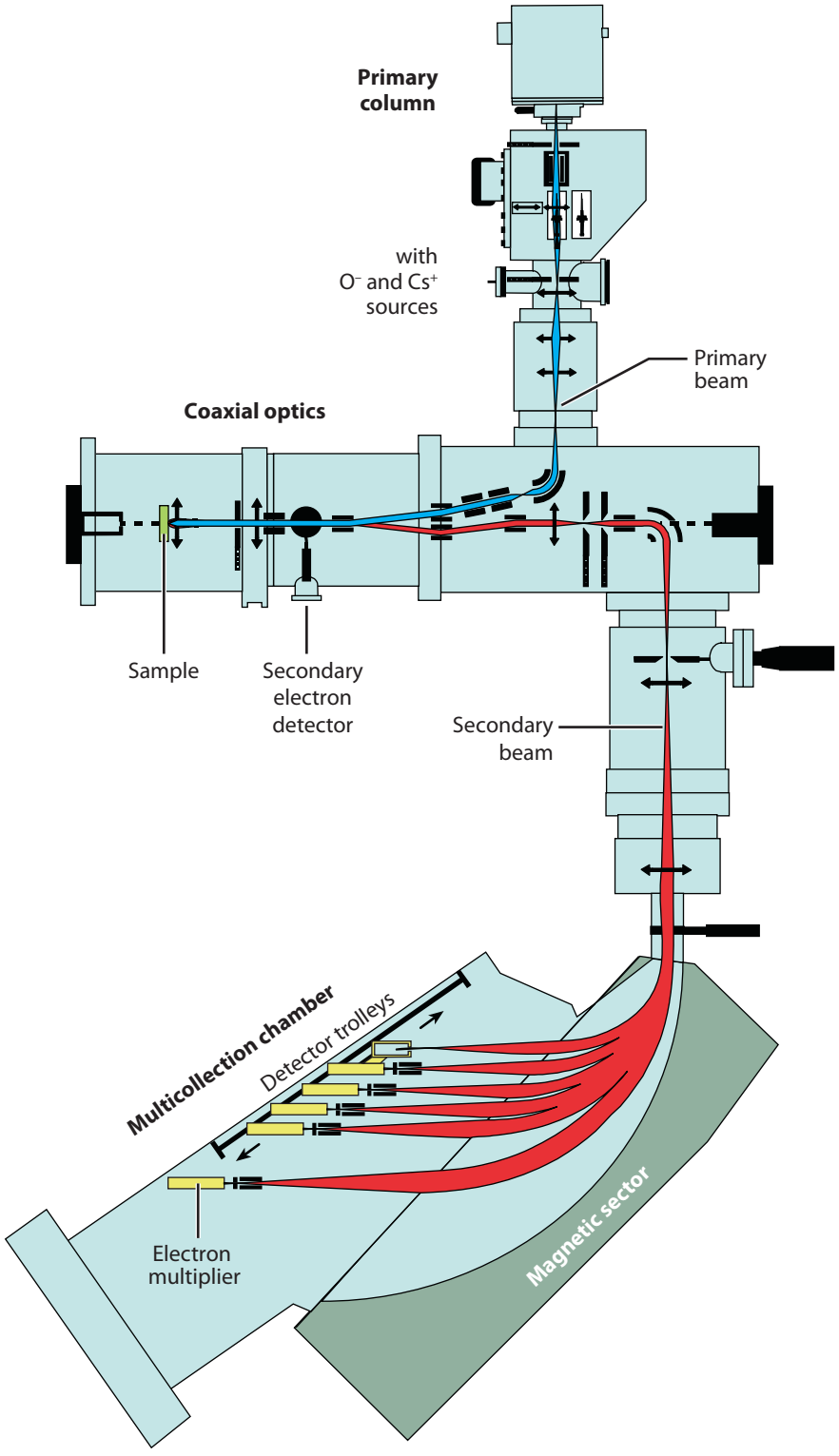

Figure 2

Schematic of the NanoSIMS 50 from CAMECA showing the major components for biological imaging. The instrument uses either an oxygen or cesium primary ion source to generate positive or negative secondary ions, respectively. The coaxial optics enable copropagation of the primary and secondary ions, which places the primary focusing optics closer to and normal to the sample, thereby reducing the spot size on the sample. Simultaneous ion detection of up to seven species is performed on electron multipliers in the multicollection chamber. This figure is adapted from Reference 16.

flight to the detector, instrument mass resolving power is determined by the ratio of the duration of secondary ion generation (primary ion pulse length) and the length of the secondary ion path. This relationship results in a tradeoff between spatial resolution at the sample and mass resolving power because the primary ion beam pulses must be compressed to increase mass resolution, which degrades the lateral resolution of the primary beam. Limitations on maximum count rates, duty cycle, and the ratio of analyzed to sputtered material can also place limits on ToF-SIMS analysis speed and sensitivity.

Dynamic SIMS

In dynamic SIMS instruments, a continuous primary ion beam generates a continuous flow of secondary ions. Typically, an oxygen primary beam (O^-, O_2^-, or O_2^+) is used to generate positive secondary ions, and a cesium primary beam (Cs^+) is used to generate negative secondary ions. These reactive primary ions implant into the sample, increasing the probability of producing positive or negative secondary ions, respectively. The development of a microcesium source by CAMECA reduced the primary spot size to less than 1 micron for dynamic SIMS instruments. The standard oxygen source, the duoplasmatron, however, has not been improved since the development of the CAMECA f-series instruments, leaving room for the development of brighter sources of electronegative primary ions (42). Positive ion imaging can be useful for probing metals in living systems (89, 109) and for tracking metabolic pathways (e.g., for Ca^{2+} and Zn^{2+}) (4, 9, 18). Negative secondary ions are formed as the fragments of organic molecules, including all common classes of biological macromolecules. For biological samples the most important atomic secondary ions, including those introduced as atom or isotopic labels, are $^1H^-$, D^-, $^{12}C^-$, $^{13}C^-$, $^{16}O^-$, $^{18}O^-$, $^{19}F^-$, $^{31}P^-$, and $^{32}S^-$; molecular secondary ions include $^{12}CH^-$, $^{13}CH^-$, $^{12}CD^-$, $^{13}CD^-$, $^{12}CH_2^-$, $^{12}C^{14}N^-$, $^{13}C^{14}N^-$, $^{12}C^{15}N^-$, and $^{13}C^{15}N^-$ ($^{13}C^{14}N^-$, 27.0064 amu, and $^{12}C^{15}N^-$, 27.0001 amu, can be distinguished). For species with the highest ionization probability, such as O^-, F^-, S^-, and CN^-, as many as 1 in 20 atoms in the sample can be detected.

In dynamic SIMS, atomic, diatomic, and larger molecular secondary ions are generated, generally in decreasing quantities. These secondary ions are separated and analyzed continuously with a modern version of the bending magnets and electric fields introduced by J.J. Thompson in the original development of the mass spectrometer. The mass spectrometers focus in both mass and energy to achieve high mass resolving power ($M/\Delta M$). Note that mass resolving power is not directly comparable between ToF-SIMS and dynamic SIMS because ToF-SIMS produces mass spectra peaks over which counts are integrated, whereas dynamic SIMS is designed to perform ion detection at a fixed dispersion on a flattop peak. These mass spectrometers produce flattop mass peaks, which enable quantification down to 1 in 1000 precision for highly abundant species. The details of the separation system depend on the target application of the instrument and determine the ultimate mass resolution. Standard dynamic SIMS instruments (e.g., the CAMECA f series) use small radius magnets, and the transmission (the fraction of collected secondary ions making it to the detector) falls off rapidly with increase in mass resolution. Large radius SIMS instruments are used to maximize transmission at high mass resolving power (full transmission at $\sim$5000 $M/\Delta M$); these instruments are typically dedicated to geochronology and high-precision isotopic analysis. The NanoSIMS achieves relatively high transmission at high mass resolution (full transmission at $\sim$2000 $M/\Delta M$) by optimizing transmission with a narrow energy window at the entrance slit to the mass spectrometer. An example of high mass resolution of secondary negative ions on the NanoSIMS is shown in **Figure 3**. For imaging, the ions are detected with high sensitivity and little background with some type of electron multiplier. Count rates are limited to less than 1 million counts per second to prevent premature aging of detectors. These instruments are

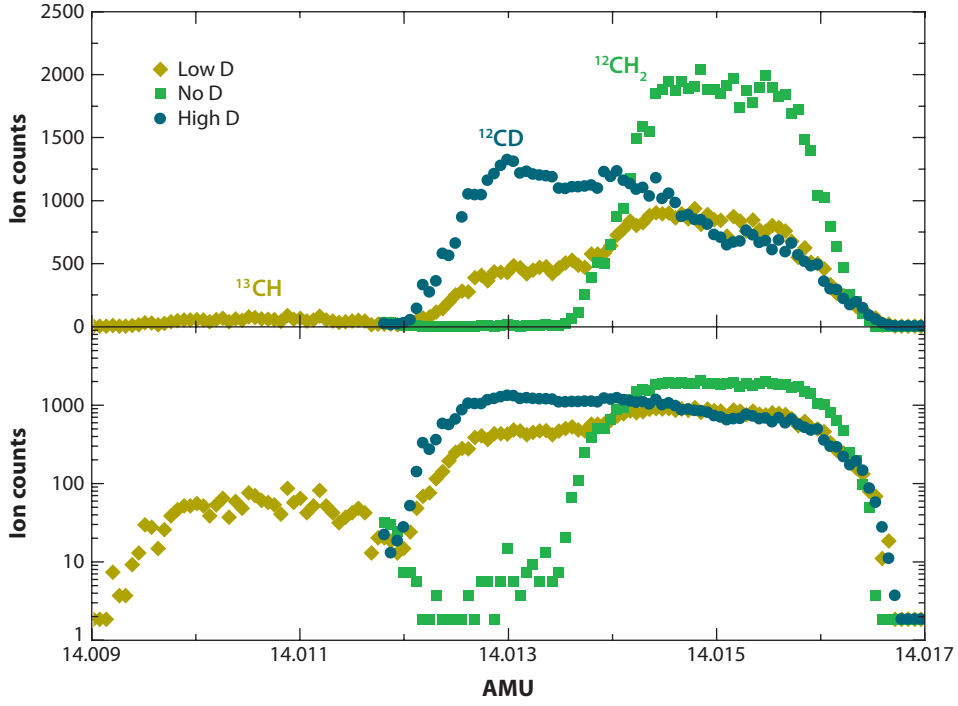

Figure 3

Mass spectra of ^{12}CD, ^{13}CH, and $^{12}CH_2$ at high mass resolving power for three different D/H ratios in spotted lipid samples, shown on linear (*upper panel*) and logarithmic scales (*lower panel*). The sample with no added D shows the peak shape with this tuning. The samples with added D show the ability to discriminate the ^{12}CD from the $^{12}CH_2$ peak by counting with the mass setting on the left side of the peak. The slope on the ^{12}CD peak top for the high D/H sample is caused by the sample being sputtered away during the mass scan. Nominal mass resolution of these scans is 8000 M/ΔM.

typically equipped with Faraday cups to enable higher secondary ion count rates, but the response time for Faraday cups is too slow for imaging.

The NanoSIMS instrument can detect five or seven secondary ions in parallel, depending on the model, so that a precise map of several different fragments detected exactly at the same location can be generated. Unlike ToF-SIMS, only preselected ions can be detected. Because biological samples are complicated mixtures and the palate of secondary ions available is limited, isotopic and/or elemental labeling that selectively discriminates the molecule(s) of interest is essential, and this has been used in most experiments reported to date. In sectioned samples, the number of ions in a given region can also be used to generate image contrast; for example, DNA produces high count rates of CN^- and P^- (60, 90).

Quantification is a central challenge for all SIMS methods. For dynamic SIMS, the species of interest are normalized to a major element in the sample of known concentration or reported as isotopic ratios. Standards that closely match the major element composition of the unknowns are analyzed under the same conditions as the unknown to control for differences in ion yield between the species of interest and the normalizing species. Differences in ion yield can be substantial (113). The same methods can be applied to ToF-SIMS molecular imaging, but at this time, quantification is not the central thrust of the work on biological samples and remains an important direction for the next generation of experiments.

SAMPLE PREPARATION

AFM: atomic force microscopy

Because imaging mass spectrometry is performed in ultrahigh vacuum, sample preparation methods that preserve the biologically relevant organization being probed are essential. As described in detail below, evaluation of sample quality with other methods prior to SIMS analysis is prudent. Regions of the sample can be examined with comparable lateral resolution by near-field methods such as atomic force microscopy (AFM) and electron microscopy, and larger regions can be compared with optical measurements. Many of the same issues arise in electron microscopy. Although some imaging mass spectrometry instruments have a provision for a cold stage, in most cases it is necessary to remove water and minimize salts. This is best achieved by rapid freezing, e.g., using liquid ethane or propane, which prevents crystallization of water, and by keeping the sample frozen while subliming off the vitreous ice. In addition to removing water, it is essential that the molecules of interest not sublime off the surface during freeze-drying or in the high-vacuum environment of the mass spectrometer, and that contamination of the surface by pump-oil or the laboratory environment should be minimized. Just as background fluorescence from a variety of sources compromises high-sensitivity fluorescence measurements, environmental contamination can be a serious problem in mass spectrometry.

Even with careful control and relatively simple samples (lipid bilayers on solid supports), we find that samples are often poorly preserved. This is best seen on a micron scale either by adding a fluorescent dye (e.g., a dye-labeled lipid for lipid monolayer or bilayer samples) or by imaging ellipsometry. The latter does not require a dye and can measure small thickness variations that may arise if the sample separates from the substrate. Prior assessment of regions that should be avoided is essential, and regions identified as interesting to probe at a later time in the imaging mass spectrometer must be found again, so combinations of imaging methods require the placement of some sort of landmark on the surface so the same region can be located with high precision. In the case of lipid bilayers on solid supports, this is readily achieved by membrane patterning (38), in which a grid pattern spacing on the order of tens of microns provides visual landmarks that can be mapped with optical techniques, such as fluorescence microscopy or imaging ellipsometry, and used to locate the same region on the surface for analysis by multiple complementary techniques, including AFM and imaging mass spectrometry.

Methods of sample preparation for cells and tissues need to be evaluated according to the experimental goals. Mapping diffusible ions requires fast freezing methods (19). Outside of this extreme case, little work has been done to determine the trade-offs between ease of sample preparation and sample integrity. Fast freezing and low temperature dehydration are generally regarded as the gold standard (19, 35, 41, 89); other methods have been used such as standard resin embedding and ultramicrotomy (60, 61), chemical fixation and air drying (65, 87), and even no treatment for stable structures such as bacterial spores (33).

NanoSIMS IMAGING OF METABOLIC PATHWAYS AND MICROBIAL COLONIES

To date only a handful of laboratories have reported results using a NanoSIMS on biological samples. This is partly because there are fewer than 20 instruments in the world and most are largely dedicated to studying hard materials. In addition, there is a significant hurdle for new entrants into the field because the instruments are complex and require extensive training to acquire meaningful data, and methods of data analysis and sample preparation are not standardized. Much of the published literature is found in relatively specialized journals that would not be routinely seen by biochemists or structural biologists, and the few higher-profile papers are the result of a great deal of effort. Much of this work is still in the method development and capability demonstration stage.

Approximately one-quarter of the publications fall in the category of studies of metabolic pathways (4, 17, 25, 40, 56, 60, 89, 90, 95). Several studies have demonstrated the value of NanoSIMS for tracer studies, including ^{13}C-labeled free fatty acid transport across cell membranes (56), thyroid uptake of iodine (17, 25), and cellular uptake and distribution of an ^{15}N-labeled peptide vector (95). Lechene et al. (60) provide an extensive exposition of the use of stable isotopes for cell biology. A recent study probes the origin of the CN^- ion based on the formation of a $^{13}C^{15}N$ cluster from adjacent ^{13}C- and ^{15}N-labeled proteins (62). This work follows an early study of the origin of the CN^- molecular ion that demonstrated that it could come directly from directly bonded atoms or from atom recombination (72). This phenomenon may potentially be exploited to obtain proximity information on a length scale much smaller than the primary beam spot size.

Applications of NanoSIMS in microbiology have expanded rapidly. NanoSIMS has been used to image the distribution of isotopic and elemental tracers at the scale of individual bacterial cells—which can be submicron in size—to infer microbial metabolism (2, 6, 20, 50, 60, 61, 65, 78, 87, 110). This application is valuable for microbiologists because microbial metabolism has typically been studied in pure cultures or inferred from genomic data, even though most microbes cannot be cultured, pure cultures may not reflect metabolism in mixed cultures, and genomic data reflect capability, not actual processes. Orphan et al. (80) were the first to use SIMS to monitor microbial metabolism in a natural consortium. They used fluorescent probes hybridized to ribosomal RNA to identify microbes in a relatively simple, spherically symmetric consortium amenable to analysis by SIMS with micron-scale lateral resolution. To determine microbial metabolism, the fluorescent probes were correlated to natural abundance isotopic analysis with a large-radius SIMS instrument. Natural abundance isotopic analysis provided insight into microbial metabolism because of the large natural fractionation in carbon isotopes by the methanogenic bacteria in the consortium. For most NanoSIMS studies, stable isotope-labeled substrates are provided to the microbial consortium to determine which microbes metabolize the substrate. The higher spatial resolution of the NanoSIMS allows individual cells and subcellular regions to be resolved, and simultaneous ion detection facilitates imaging of stable isotope analysis and elementally tagged molecular probes within single micron-scale cells (6, 65, 78).

NanoSIMS has also been used to characterize microbially mediated geochemical processes using isotopic tracers (27), natural abundance stable isotopes (28), and organic nitrogen detection and mapping in mineral aggregates (77). Other biologically related geochemistry studies include elemental mapping and tracer studies on reef-building corals (20, 75), statoliths (118), coccoliths (36, 92), diatoms (2), and fossil organic mapping (79).

IMAGING MASS SPECTROMETRY OF BIOLOGICAL MEMBRANES

Although the lipid bilayer is the universal structural element of biological membranes, relatively little is known about the lateral organization of lipids and membrane-associated proteins. Biological membranes are highly dynamic as lipids generally diffuse in the plane of the membrane, as do many membrane-associated proteins. Specific associations among lipids such as sphingomyelin, cholesterol, and membrane-anchored proteins, often called lipid rafts, are hypothesized to form an organized entity with collective function. These microdomains are believed to play a central role in organizing this fluid system, enabling the cell membrane to carry out essential cellular processes, including protein recruitment and signal transduction (43, 117). Yet direct visualization of these microdomains has proved to be difficult, the precise compositions and other physical characteristics of these domains have not been established, and thus the existence of rafts is controversial (24).

There has been extensive work on lateral phase separation using model membranes, such

POPC: 1-palmitoyl-2-oleoylphosphatidylcholine

as monolayers at the air-water interface or on hydrophobic supports, and bilayers, either on solid supports or in giant vesicles. Domains are often visualized by the partitioning of fluorescent probes between phases. Although many dye-labeled lipids are available, their physical properties can be different from those of native lipids, which is not surprising because the dyes are often covalently attached via important functional groups and they introduce unnatural charge and functionality. Imaging mass spectrometry has the potential to make a major contribution to this field by directly imaging the lateral distributions of components within the membrane without changing the chemical structures of the components of interest, and therefore the delicate interactions that are essential for function are not perturbed. ToF-SIMS has been used to directly detect and image various membrane components in synthetic model membrane systems, biological tissues, and individual cell membranes on the length scale of 200 nm–1 μm. Dynamic SIMS performed with the NanoSIMS has been combined with isotopic labeling of specific components to extract comparable information from supported lipid bilayers on a scale of 100 nm. In this section, we review this work.

ToF-SIMS

The majority of SIMS analysis of lipid membranes has been performed using ToF-SIMS. Because large molecular fragments often have distinctive masses, labeling is, in principle, not required for component identification. Winograd and coworkers (74, 102) have pioneered the ToF-SIMS analysis of domain formation in Langmuir-Blodgett lipid monolayers deposited onto self-assembled monolayers of alkane thiols on gold. To date, data have been reported at the 1 μm length scale; although a primary ion beam diameter of 100–200 nm can be achieved, the lateral resolution of these studies was limited by the pixel size. This body of work was discussed in a recent review of ToF-SIMS imaging of lipid membranes (54), so we only briefly summarize key results here.

ToF-SIMS analysis of biological and synthetic lipid membranes offers the advantages that unlabeled model or native cell membrane samples can be characterized, and the resulting mass spectra contain a wealth of information on the molecules present even if they were unidentified at the time of analysis. A prime example of the strengths of ToF-SIMS is demonstrated in a recent report characterizing an unlabeled lipid monolayer composed of sphingomyelin (m/z 731 and m/z 264), cholesterol (m/z 385 and m/z 369), and a partially unsaturated lipid [1-palmitoyl-2-oleoylphosphatidylcholine (POPC), m/z 760 and m/z 224] with 1 μm lateral resolution (74). The distributions of the characteristic secondary ions revealed domains enriched with sphingomyelin and cholesterol but deficient in POPC (74). ToF-SIMS has also been used to image phase separation within lipid monolayers that model lung surfactants (44) and contain a surfactant protein (10, 12) with 200 nm–1 μm lateral resolution.

The ability to directly image the lateral distributions of unlabeled molecular components within a sample renders ToF-SIMS an ideal method to image lipid distribution in actual cell membranes. There are several reports of imaging the distributions of membrane components within biological tissues and individual cells with a lateral resolution of one to a few microns (1, 21, 83, 85, 93, 94, 99, 106, 107). The most impressive example of the potential of this method is a report from Ostrowski et al. (82), who demonstrate a decreased abundance of phosphatidylcholine and an increase in an aminoethylphosphonolipid detected at the plasma membrane sites of fusion between *Tetrahymena* cells. If this result can be generalized, it can provide a unique opportunity to analyze the composition of specific regions of membranes that are important in other cellular processes.

The primary issues for ToF-SIMS analysis of biological samples are sensitivity, spatial resolution, specificity, and quantification. Unfortunately, the high-mass fragment ions used for component identification often have low yields. The further development of polyatomic

primary ion sources is a promising approach to decrease molecular fragmentation and increase the yields of molecular ions and high-mass molecular fragment ions, thereby simplifying component identification and increasing the working lateral resolution (29, 81). Molecular fragment identification can be challenging for complex samples, and in some cases, high-mass molecular fragment ions are not uniquely characteristic of a single membrane component (102), so selective deuterium labeling may also be required for component identification (8). The central challenge for quantification is determining the relationship between secondary ion signal intensity and component concentration. This relationship is subject to matrix effects that result in differences in ion yields. For example, the yields of ToF-SIMS secondary ions can vary because of changes in the lipid packing density in the monolayer (11, 73) and other differences in the local membrane environment (84, 88). These complications can be mitigated by using relative sensitivity factors measured on calibration samples (74). Furthermore, the yields of large molecules are often low and may be different for different molecules (e.g., lipids versus proteins, phospholipids versus cholesterol), limiting sensitivity and compromising quantification. Though beyond the scope of this review, multivariate analysis techniques that glean component identity from the abundant low-mass fragment ions that are otherwise unexploited can also improve component identification (108). ToF-SIMS is especially powerful for detecting lateral variations that give rise to visible contrast in the component-specific ion image, although care must be taken in translating this change in the signal intensity into variations in the abundance of a specific species, as opposed to changes in the local environment that alter the secondary ion yield.

Dynamic SIMS

In contrast to ToF-SIMS, only tiny molecular fragments such as atomic and diatomic secondary ions are detected in dynamic SIMS analysis. Therefore the incorporation of distinct stable isotopes or unique atoms (e.g., F) into the components of interest is required for component identification. Isotopically labeled molecules and the corresponding unlabeled molecules have identical chemical structures, and much of what we know about biochemical pathways is derived from studies that use stable and radioactive isotopes as tracers. As described in the section on instrumentation, while ToF-SIMS generates an entire mass spectrum, dynamic SIMS performed with the NanoSIMS only allows the parallel detection of five or seven different m/z ratios (depending on the NanoSIMS model). The trade-off is that a higher spatial resolution and greater sensitivity to small mol fractions of each component can be achieved by this approach than by ToF-SIMS. Taken together, dynamic SIMS performed with the NanoSIMS is advantageous when the components of interest can be isotopically labeled and when high lateral resolution and sensitivity are the primary goals. To date, a direct comparison of ToF-SIMS and NanoSIMS images for identically prepared samples has not been reported. This would provide a useful assessment of the strengths of each approach.

Model lipid membranes are an ideal test bed for dynamic SIMS because they have been characterized by many surface-sensitive methods and isotopic labels can be easily incorporated. Our joint published work to date focuses on supported lipid bilayers, one of the simplest model systems that captures essential features of biological membranes (31, 57, 58). At the time we began this work, it was not clear that the sensitivity would be sufficient to detect a single bilayer using the NanoSIMS, let alone to attempt quantitative analysis with high spatial resolution. Furthermore, there was no precedent for preparing supported bilayers for high vacuum analysis, and our initial efforts often led to surfaces that, when imaged by adding a small amount of a fluorescent dye-labeled lipid, were of poor quality.

Supported lipid bilayers are prepared by exposing glass or silica surfaces to a suspension of lipid vesicles. This self-assembly process does

DLPC: 1,2-dilauroylphosphatidylcholine

DSPC: 1,2-distearoylphosphatidylcholine

not occur on many materials, and by placing such materials on substrates as barriers, bilayer assembly can be directed only to those regions where the glass or silica is exposed. This is called membrane patterning, and many methods for varying and manipulating the composition of lipid and membrane-associated protein components in these patterned surfaces have been developed (37). Although supported bilayers can be formed on the native SiO_2 that forms spontaneously on Si in air, bilayers on native oxide are not particularly stable. By growing a thicker but still very thin SiO_2 layer on the Si substrates, stable bilayers can routinely be formed, and these SiO_2 layers can be patterned with other materials (we currently use Cr) so that bilayer regions on the surface can be relocated by different imaging methods such as fluorescence, ellipsometry, AFM, and ultimately the NanoSIMS (which destroys the sample).

We use 5 × 5 mm Si wafers, which are held firmly and grounded in our NanoSIMS sample holders. The oxide thickness on these wafers is important because charge buildup on the surface during exposure to the Cs^+ beam can reduce the ion yield and resolution, so a compromise between SiO_2/bilayer stability and charge dissipation through the grounded Si wafer must be sought. Although a comprehensive analysis has not been performed, it appears that a roughly 10-nm-thick SiO_2 layer is a good compromise, which is consistent with the mean implantation depth of 20 nm for the 16 kV Cs^+ primary ions.

This thin oxide layer has a second consequence for fluorescence imaging. Because the underlying Si substrate is an excellent mirror, incoming light is reflected off the surface and interferes, giving a standing wave pattern above the substrate with a null at the surface, a maximum at one-quarter of the wavelength of light, a null again at one-half the wavelength of light and so on [this is the basis of the interferometric technique fluorescence inference contrast microscopy (59)]. Because the SiO_2 layer is very thin, fluorescence from molecules in a bilayer that are only a few more nanometers from the Si mirror is very weak. After freeze-drying, the molecules are likely even closer to the mirror, and we also find that what little fluorescence there is rapidly photobleaches in air. Thus, although a thin SiO_2 layer is optimal for the NanoSIMS measurement, it makes conventional epifluorescence microscopy more difficult.

Preserving the bilayer and its lateral organization on the surface by freeze-drying is a tricky process. Supported bilayers are not stable when exposed to air, so the sample must be under water at all times, but the amount of water must be kept to a minimum for rapid freezing (the 1-mm-thick Si wafer also presents a substantial thermal mass). The sample is rapidly immersed in liquid ethane with a minimal perturbation of the surface and then transferred under liquid nitrogen into a freeze-drying chamber where the water is removed at low temperature (we use an oil-free scroll pump to minimize contamination). Once freeze-dried, the surfaces appear to be stable for a long time, e.g., domains visualized by fluorescence microscopy (necessarily microns or larger) are preserved pre- and postfreeze-drying and remain for long periods. Although lipid mobility is a hallmark of biological membranes, once freeze-dried this mobility ceases. Also, because the sample is frozen in a small fraction of a second, a typical lipid molecule with a diffusion coefficient of approximately 1 $\mu m^2\ s^{-1}$ will at most exchange positions with only a few neighbors, and this is much less than the lateral resolution of the NanoSIMS measurement due to the diameter of the primary ion beam.

As a step toward the ultimate goal of high-resolution membrane composition analysis, we have demonstrated that small domains within a phase-separated lipid bilayer could be imaged with 100-nm lateral resolution and that the lipid composition within small regions of the membrane could be quantified by NanoSIMS imaging (58). Homogeneous bilayers composed of 1,2-dilauroylphosphatidylcholine-^{15}N (^{15}N-DLPC), 1,2-distearoylphosphatidylcholine-$^{13}C_{18}$ ($^{13}C_{18}$-DSPC), and 0.5 mol% of a

fluorescent lipid that enabled the bilayer to be visualized by fluorescence microscopy during sample preparation were formed by vesicle fusion on chrome-patterned silicon substrates at a temperature at which both lipids were in the fluid state. Pure DSPC has a gel-to-liquid phase transition temperature of 55°C, and pure DLPC has a gel-to-liquid phase transition temperature of –1°C. The freely mixed supported bilayers were cooled to induce phase separation due to this difference in their phase behavior associated with acyl chain lengths. The bilayers were flash-frozen and freeze-dried to remove the water without perturbing the bilayer's organization, and the locations and geometries of the gel and fluid phases within the freeze-dried lipid bilayer were imaged by AFM (**Figure 4*d***). The height difference between these two phases was consistent with measurements made on hydrated, phase-separated bilayers composed of DSPC and DLPC (67).

The $^{13}C^{1}H^{-}$ and $^{12}C^{15}N^{-}$ secondary ion signals were used to visualize the $^{13}C_{18}$-DSPC and ^{15}N-DLPC distributions, respectively, within the lipid membrane. The lipid-specific secondary ion images showed that domains enriched with $^{13}C_{18}$-DSPC, as evidenced by a locally elevated $^{13}C^{1}H^{-}$ signal and decreased $^{12}C^{15}N^{-}$ signal, were dispersed within a ^{15}N-DLPC–rich bilayer (**Figure 4**). The positions and geometries of the $^{13}C_{18}$-DSPC–enriched domains visualized by the NanoSIMS were nearly identical to the gel phase domains imaged by AFM. A few features in the AFM image did not produce lipid-specific secondary ions (**Figure 4**); the height difference between these objects and the bilayer (>5 nm) verified that these objects were unlabeled debris, not lipid domains. This side-by-side comparison is particularly important because AFM and NanoSIMS images contain different information and each enhances the value of the other.

Quantitative information on the lipid composition within small regions of the membrane was obtained by calibrating the lipid-specific secondary ion signal intensities with standard samples. To establish the calibration curves, two sets of homogeneous supported lipid bilayer samples that each systematically varied in the $^{13}C_{18}$-DSPC or ^{15}N-DLPC content were made. Using the NanoSIMS, measurements were made on each calibration sample within the two sets. The normalized $^{13}C^{1}H^{-}$ or $^{12}C^{15}N^{-}$ signal intensities ($^{13}C^{1}H^{-}/^{12}C^{-}$ or $^{12}C^{15}N^{-}/^{12}C^{-}$) were determined at several regions in each calibration sample, and the standard deviation relative to the average $^{13}C^{1}H^{-}$ or $^{12}C^{15}N^{-}$ signal intensity measured on each sample was below 3% and 5%, respectively. Calibration curves were constructed from this data, and the normalized $^{13}C^{1}H^{-}$ and $^{12}C^{15}N^{-}$ signal intensities had excellent linear correlations with the isotopic enrichment in the bilayer, which suggests that matrix effects were negligible in these samples. The normalized $^{12}C^{15}N^{-}$ signal intensity was sensitive to the thickness of the SiO_2 layer of the substrate that supported the lipid membrane, so the SiO_2 thickness used for these experiments varied <1 nm. The magnitude of matrix effects within bilayer samples that contain more diverse membrane compositions is currently being investigated.

Using these calibration curves, the gel and fluid phase compositions were evaluated by converting the component-specific secondary ion signal intensities collected from small regions of the bilayer into mol% concentrations (**Figure 5**). Most of the gel phase domains consisted of a ~9:1 molar ratio of $^{13}C_{18}$-DSPC to ^{15}N-DLPC, consistent with the phase diagram for this mixture. A statistically significant elevation in the amount of ^{15}N-DLPC was detected at a localized area in one gel phase domain. Inspection of the AFM image acquired at this location revealed that the elevated ^{15}N-DLPC concentration within the domain corresponded to a small (<200-nm-diameter) depression in the thickness of the domain, and this could be interpreted as a fluid phase subdomain trapped within the gel phase (**Figure 5**). In the bilayer regions that corresponded to the fluid phase, the molar ratio of ^{15}N-DLPC to $^{13}C_{18}$-DSPC was greater than 19:1, again consistent with the

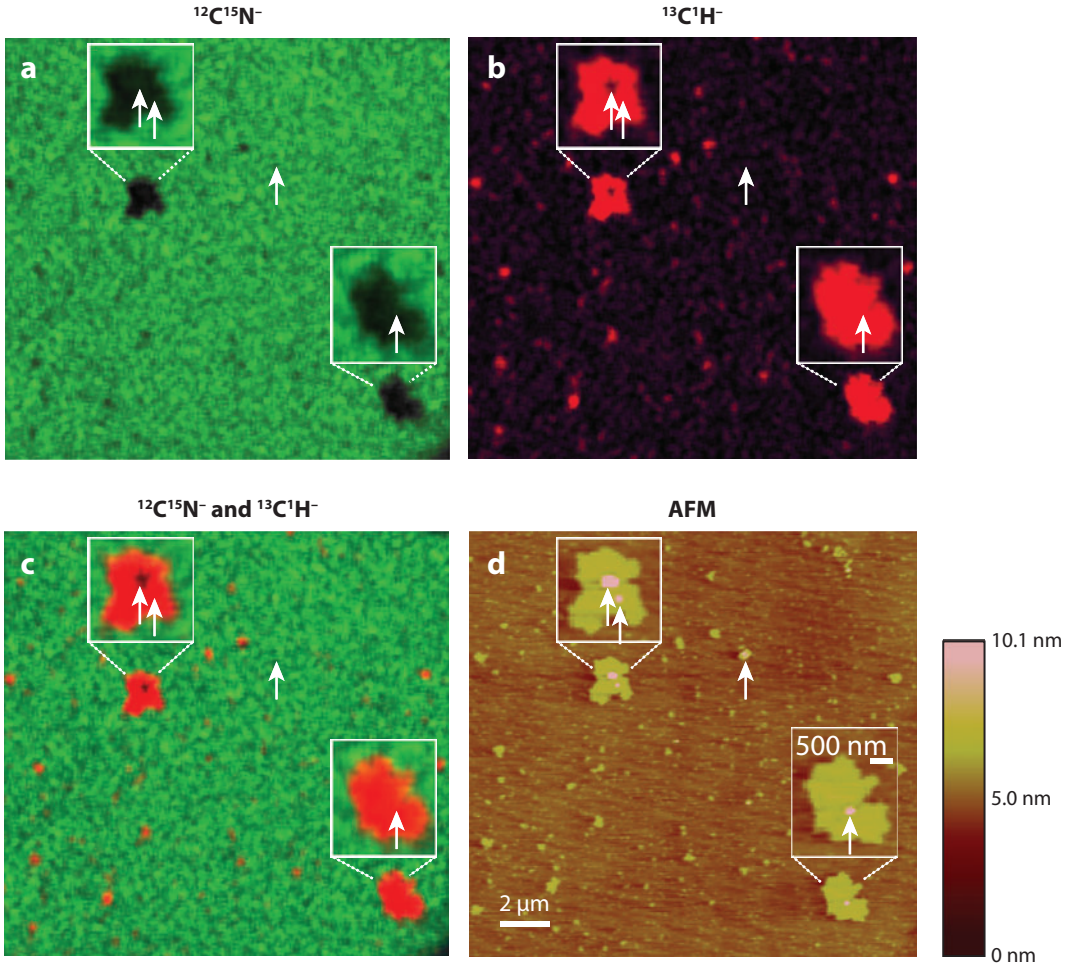

Figure 4

NanoSIMS analysis of a freeze-dried, phase-separated supported lipid bilayer composed of 1,2-dilauroylphosphatidylcholine-^{15}N (^{15}N-DLPC) and 1,2-distearoylphosphatidylcholine-$^{13}C_{18}$ ($^{13}C_{18}$-DSPC) (*a–c*) and the atomic force microscopy (AFM) image of the topography of the same bilayer location (*d*). The analysis was performed with the NanoSIMS 50 using a cesium primary ion beam with a diameter of 100 nm and a pixel size of 100 × 100 nm. (*a*) The normalized $^{12}C^{15}N^-$ secondary ion signal intensity (*green*) reveals the distribution of ^{15}N-DLPC in this area, and (*b*) the normalized $^{13}C^1H^-$ secondary ion signal (*red*) shows the distribution of $^{13}C_{18}$-DSPC in the membrane. (*c*) Overlay of the two lipid-specific ion signals. A comparison of the AFM image (*d*) of the membrane topography that was acquired at the same sample location prior to SIMS analysis to the lipid-specific secondary ion images (*a–c*) shows that the sizes and shapes of the $^{13}C_{18}$-DSPC–enriched lipid domains visualized by SIMS are nearly identical to the gel phase domains imaged by AFM. Arrows indicate objects in the AFM image that are unlabeled debris, not labeled domains, and their locations in the SIMS images.

phase diagram. For 300 × 300 nm^2 bilayer regions, the uncertainty in the lipid composition was under 10%, although uncertainties as large as 20% were occasionally measured. The uncertainty in the estimation of lipid composition is based on counting statistics, as described in detail in the supplementary information of our previous report (58).

This work validates the ability to image the distribution of membrane components on the submicron length scale that is relevant to organization within biological membranes.

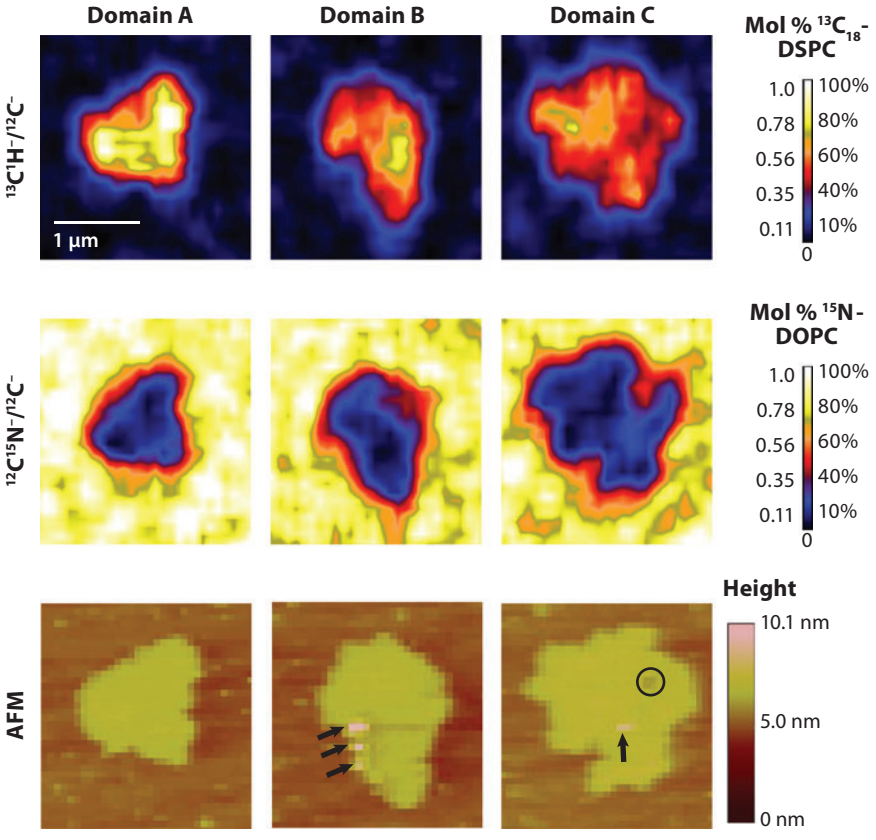

Figure 5

Quantitative analysis of membrane domains as described in **Figure 4**. The normalized $^{13}C^1H^-$ and $^{12}C^{15}N^-$ secondary ion signal intensities were calibrated using sets of homogeneous lipid bilayers that systematically varied in isotopic composition. The thermal false color scales represent the abundance of 1,2-distearoylphosphatidylcholine-$^{13}C_{18}$ ($^{13}C_{18}$-DSPC) and 1,2-dilauroylphosphatidylcholine-^{15}N (^{15}N-DLPC) within the bilayer. AFM images acquired at the same locations before SIMS analysis reveal topography. Lower concentrations of both lipids were detected in the locations where debris was identified by AFM (*arrows*). The lipid composition within the gel phase was typically ~9:1, $^{13}C_{18}$-DSPC to ^{15}N-DLPC (domain A), but unusually high amounts of ^{15}N-DLPC were occasionally detected within the gel phase domains (domains B and C). AFM imaging indicated a small (<200-nm-diameter) depression that might indicate that a small fluid phase domain (*circle*) was entrapped within the gel phase (domain C). The presence of this fluid phase subdomain is confirmed by the NanoSIMS image, which reveals a locally elevated concentration of ^{15}N-DLPC at this location. SIMS images were acquired with the NanoSIMS 50. Pixel size is 100 × 100 nm, and the images are smoothed over three pixels.

NanoSIMS analysis of actual cell membranes has not yet been attempted. The obvious challenges will be to selectively incorporate distinct stable isotopes into the components of interest and to isolate the cell membrane intact for analysis. Methods for achieving this have been reported, mostly for fluorescence imaging (23, 86).

COMPARISON WITH OTHER ADVANCED IMAGING METHODS

There are many approaches to imaging biological systems, depending on the nature of the samples, in particular whether they are alive, fixed, or otherwise preserved and/or sectioned, the length scale, sensitivity, and type of

information that can be extracted. We close this review with a brief comparison of imaging mass spectrometry to a few methods that have seen great recent advances. It is our strong belief that combinations of methods are the best approach; that is, these are not competing, but complementary. An excellent example is provided by the NanoSIMS images of phase-separated supported bilayers compared with AFM images in **Figure 4**. AFM is a well-established method that can provide atomic resolution topographical images of the surface of hard and soft objects under ideal conditions, but not chemical information [although a recent example with a functionalized AFM tip shows the potential for molecule-specific information (111)]. The NanoSIMS data contain little topographic information but provide unambiguous identification of isotopic composition that translates into chemical identification. The spatial resolution (both lateral and vertical) is much poorer than with AFM, but the molecular information content is much greater; thus side-by-side measurements on the same sample are much more powerful than either alone. Another comparative example probing the architecture of pathogen cell walls has been reported recently (22).

Cryo-electron microscopy is a powerful tool for imaging complex assemblies such as the ribosome, microtubules, and nuclear pores, to name a few spectacular examples (30, 103). Advances in electron microscopes and image processing open the possibility of nearly atomic-level resolution for noncrystalline samples. At the same time, advances in image reconstruction and thin sectioning combined with state-of-the-art electron microscopy make electron tomography a reality (39, 68, 96). Each of these approaches, like mass spectrometry imaging, depends upon careful sample preservation. Molecule-specific information can be obtained by affinity labels that are typically conjugated to large metal clusters, which is a disadvantage compared with the intrinsically multiplexed mass-specific information of mass spectrometry. As with imaging mass spectrometry, these techniques are still limited to a few laboratories, as the instrumentation and expertise are specialized, and results emerge slowly. The potential for side-by-side comparisons of imaging mass spectrometry and electron tomography is particularly attractive.

Commercial light microscopes come equipped with extraordinary optics, detection systems, and software, so that advanced methods of data acquisition and analysis have become routine. Traditional approaches to sample staining with dyes or dye-labeled antibodies have been supplemented by genetically encoded labels based on green fluorescent protein (34). The advantage of these approaches, especially using green fluorescent protein, is that measurements can be performed on living samples and single molecules can be detected due to the extreme sensitivity of fluorescence detection (76). The obvious limitations for imaging the organization of complex systems are the need for specific labels (one only sees what is labeled with a fluorescent tag), the label may interfere with an important interaction, and the diffraction limit (on the order of several hundred nanometers under ideal conditions). The last limitation has been challenged by a series of increasingly impressive methods. Most of these approaches involve some sort of structured illumination. Near-field scanning optical microscopy scans a subdiffraction-sized aperture over the sample (45). Structured illumination near nonbiological surfaces can be achieved by evanescent wave approaches, in which the light field decays exponentially from a surface with a higher refractive index than the material being probed (e.g., total internal reflection fluorescence microscopy) (3), or by interference contrast, in which a standing wave is created near a reflective surface (e.g., fluorescence interference contrast microscopy) (59). Most impressive and potentially most general are methods that create structured illumination using the microscope optics or exploit the photophysical processes of the fluorescent molecules used for imaging to obtain resolution much below the diffraction limit. In particular the works of Hell and coworkers (46, 47, 55, 97, 98, 112) have demonstrated resolution better than 100 nm.

These state-of-the-art methods are not yet routine, and in most cases the images take considerable time to obtain, but they can be applied to intact three-dimensional objects. Finally, a new class of super-resolution methods based on the location of individual molecules and complex photophysics have recently been developed that avoid structured illumination but typically require multiple labels (5, 7, 52). These methods are evolving rapidly and offer spatial resolution that is comparable to imaging mass spectrometry. While the sensitivity is at the level of individual molecules, multiplexed detection and identification are limited to what is labeled.

Although fluorescence microscopy is widely used because the instrumentation and labels are so readily available, infrared microscopy can provide spectral signatures of specific types of molecules based on the characteristic vibrational spectra of the molecules in the sample. In this sense, infrared-based methods parallel imaging mass spectrometry in that they give chemically specific information. The advantage is that these methods, like fluorescence microscopy, can be applied to live cells. The disadvantages are the diffraction limit (on the order of several microns for typical vibrational frequencies), sensitivity (infrared transitions are typically detected much less sensitively than electronic transitions are), and background absorption, e.g., from bulk water. Raman microscopy can be used to avoid the last, but it is quite insensitive. Coherent anti-Stokes Raman scattering can improve the sensitivity by many orders of magnitude, and this is currently being developed as a microscopy method in several laboratories (26, 64).

Each of these advanced imaging methods offers specific advantages and none provides a complete story by itself. For planar samples like model membranes, imaging mass spectrometry combined with AFM takes optimum advantage of both. For complex topologies or where fast reorganization is important for function, these methods are much less useful, although it may prove possible to trap intermediates by freezing and obtain planar images by thin sectioning. Ultimately, mass spectrometry offers the highest level of information because it is mass specific, so the future of this approach appears to be bright.

DISCLOSURE STATEMENT

The authors are not aware of any biases that might be perceived as affecting the objectivity of this review.

ACKNOWLEDGMENTS

We thank Ian Hutcheon, Nick Winograd, Francois Hillion, and Francois Horreard for many useful discussions. M.L.K. was supported by an NIH NRSA fellowship while at Stanford and holds a Career Award at the Scientific Interface from the Burroughs Wellcome Fund. This work is supported by grants from the NSF Biophysics program and NIH GM06930 (S.G.B.) and from the LLNL Lab Directed Research and Development Program and DOE Genomes to Life Program (P.K.W.) and was performed under the auspices of the U.S. Department of Energy under contract DE-AC52-07NA27344. We are grateful to the Stanford Nanofabrication Facility for fabrication and the NSF MRSEC CPIMA for analysis (ellipsometry and AFM).

LITERATURE CITED

1. Altelaar AFM, Klinkert I, de Lange RPJ, Adan RAH, Heeren RMA, Piersma SR. 2006. Gold-enhanced biomolecular surface imaging of cells and tissue by SIMS and MALDI mass spectrometry. *Anal. Chem.* 78:734–42

2. Audinot JN, Guignard C, Migeon HN, Hoffmann L. 2006. Study of the mechanism of diatom cell division by means of Si-29 isotope tracing. *Appl. Surf. Sci.* 252:6813–15
3. Axelrod D. 2001. Total internal reflection fluorescence microscopy in cell biology. *Traffic* 2:764–74
4. Azari F, Vali H, Guerquin-Kern J-L, Wu T-D, Croisy A, et al. 2008. Intracellular precipitation of hydroxyapatite mineral and implications for pathologic calcification. *J. Struct. Biol.* 162:468–79
5. Bates M, Huang B, Dempsey GT, Zhuang X. 2007. Multicolor super-resolution imaging with photo-switchable fluorescent probes. *Science* 317:1749–53
6. Behrens S, Losekann T, Pett-Ridge J, Weber PK, Ng WO, et al. 2008. Linking microbial phylogeny to metabolic activity at the single-cell level by using enhanced element labeling-catalyzed reporter deposition fluorescence in situ hybridization (EL-FISH) and NanoSIMS. *Appl. Environ. Microbiol.* 74:3143–50
7. Betzig E, Patterson GH, Sougrat R, Lindwasser OW, Olenych S, et al. 2006. Imaging intracellular fluorescent proteins at nanometer resolution. *Science* 313:1642–45
8. Biesinger MC, Miller DJ, Harbottle RR, Possmayer F, McIntyre NS, Petersen NO. 2006. Imaging lipid distributions in model monolayers by ToF-SIMS with selectively deuterated components and principal components analysis. *Appl. Surf. Sci.* 252:6957–65
9. Bordat C, Guerquin-Kern J-L, Lieberherr M, Cournot G. 2004. Direct visualization of intracellular calcium in rat osteoblasts by energy-filtering transmission electron microscopy. *Histochem. Cell Biol.* 121:31–38
10. Bourdos N, Kollmer F, Benninghoven A, Ross M, Sieber M, Galla H-J. 2000. Analysis of lung surfactant model systems with time-of-flight secondary ion mass spectrometry. *Biophys. J.* 79:357–69
11. Bourdos N, Kollmer F, Benninghoven A, Sieber M, Galla H-J. 2000. Imaging of domain structures in a one-component lipid monolayer by time-of-flight secondary ion mass spectrometry. *Langmuir* 16:1481–84
12. Breitenstein D, Batenburg JJ, Hagenhoff B, Galla H-J. 2006. Lipid specificity of surfactant protein B studied by time-of-flight secondary ion mass spectrometry. *Biophys. J.* 91:1347–56
13. Brunelle A, Touboul D, Laprévote O. 2005. Biological tissue imaging with time-of-flight secondary ion mass spectrometry and cluster ion sources. *J. Mass Spectrom.* 40:985–99
14. Burnum KE, Frappier SL, Caprioli RM. 2008. Matrix-assisted laser desorption/ionization imaging mass spectrometry for the investigation of proteins and peptides. *Annu. Rev. Anal. Chem.* 1:689–705
15. Caldwell RL, Caprioli RM. 2005. Tissue profiling by mass spectrometry: a review of methodology and applications. *Mol. Cell Proteomics* 4:394–401
16. CAMECA. 2008. *NanoSIMS 50/50L. SIMS microprobe for ultra fine feature analysis*. **http://www.cameca.fr/html/product_nanosims.html**
17. Champion C, Elbast M, Wu TD, Colas-Linhart N. 2007. Thyroid cell irradiation by radioiodines: a new Monte Carlo electron track-structure code. *Braz. Arch. Biol. Technol.* 50:135–44
18. Chandra S. 2004. Subcellular SIMS imaging of isotopically labeled amino acids in cryogenically prepared cells. *Appl. Surf. Sci.* 231–232:462–66
19. Chandra S, Morrison GH. 1992. Sample preparation of animal tissues and cell cultures for secondary ion mass spectrometry (SIMS) microscopy. *Biol. Cell* 74:31–42
20. Clode PL, Stern RA, Marshall AT. 2007. Subcellular imaging of isotopically labeled carbon compounds in a biological sample by ion microprobe (NanoSIMS). *Microsc. Res. Tech.* 70:220–29
21. Colliver TL, Brummel CL, Pachloski ML, Swanek FD, Ewing AG, Winograd N. 1997. Atomic and molecular imaging at the single-cell level with TOF-SIMS. *Anal. Chem.* 69:2225–31
22. Dague E, Delcorte A, Latge J-P, Dufrene YF. 2008. Combined use of atomic force microscopy, X-ray photoelectron spectroscopy, and secondary ion mass spectrometry for cell surface analysis. *Langmuir* 24:2955–59
23. Danelon C, Perez JB, Santschi C, Brugger J, Vogel H. 2006. Cell membranes suspended across nanoaperture arrays. *Langmuir* 22:22–25
24. Edidin M. 2003. The state of lipid rafts: from model membranes to cells. *Annu. Rev. Biophys. Biomol. Struct.* 32:257–83
25. Elbast M, Wu TD, Guiraud-Vitaux F, Guerquin-Kern JL, Petiet A, et al. 2007. Kinetics of intracolloidal iodine in thyroid of iodine-deficient or equilibrated newborn rats. Direct imaging using secondary ion mass spectrometry. *Cell Mol. Biol.* 53(Suppl.):OL1018–24

26. Evans CL, Xie XS. 2008. Coherent anti-stokes Raman scattering microscopy: chemically selective imaging for biology and medicine. *Annu. Rev. Anal. Chem.* 1:883–909
27. Fayek M, Utsunomiya S, Pfiffner SM, White DC, Riciputi LR, et al. 2005. The application of HRTEM techniques and NanoSIMS to chemically and isotopically characterize *Geobacter sulfurreducens* surfaces. *Can. Mineral.* 43:1631–41
28. Fike DA, Gammon CL, Ziebis W, Orphan VJ. 2008. Micron-scale mapping of sulfur cycling across the oxycline of a cyanobacterial mat: a paired NanoSIMS and CARD-FISH approach. *ISME J.* 2:749–59
29. Fletcher JS, Lockyer NP, Vickerman JC. 2006. C60, Buckminsterfullerene: its impact on biological ToF-SIMS analysis. *Surf. Interface Anal.* 38:1393–400
30. Frank J. 2006. *Three-Dimensional Electron Microscopy of Macromolecular Assemblies*. New York: Oxford Univ. Press
31. Galli Marxer C, Kraft ML, Weber PK, Hutcheon ID, Boxer SG. 2005. Supported membrane composition analysis by secondary ion mass spectrometry with high lateral resolution. *Biophys. J.* 88:2965–75
32. Garrison BJ, Postawa Z. 2008. Computational view of surface based organic mass spectrometry. *Mass Spectrom. Rev.* 27:289–351
33. Ghosal S, Fallon SJ, Leighton T, Wheeler KE, Hutcheon ID, Weber PK. 2008. Imaging and 3D elemental characterization of intact bacterial spores with high-resolution secondary ion mass spectrometry (NanoSIMS) depth profile analysis. *Anal. Chem.* 80:5986–92
34. Giepmans BNG, Adams SR, Ellisman MH, Tsien RY. 2006. The fluorescent toolbox for assessing protein location and function. *Science* 312:217–24
35. Grignon N. 2007. Using SIMS and MIMS in biological materials. In *Electron Microscopy: Methods and Protocols*, ed. J Juo, pp. 569–91. Totowa, NJ: Humana Press Inc.
36. Grovenor CRM, Smart KE, Kilburn MR, Shore B, Dilworth JR, et al. 2006. Specimen preparation for NanoSIMS analysis of biological materials. *Appl. Surf. Sci.* 252:6917–24
37. Groves JT, Boxer SG. 2002. Micropattern formation in supported lipid membranes. *Acc. Chem. Res.* 35:149–57
38. Groves JT, Ulman N, Boxer SG. 1997. Micropatterning fluid lipid bilayers on solid supports. *Science* 275:651–53
39. Gruska M, Medalia O, Baumeister W, Leis A. 2008. Electron tomography of vitreous sections from cultured mammalian cells. *J. Struct. Biol.* 161:384–92
40. Guerquin-Kern J-L, Hillion F, Madelmont J-C, Labarre P, Papon J, Croisy A. 2004. Ultra-structural cell distribution of the melanoma marker iodobenzamide: improved potentiality of SIMS imaging in life sciences. *Biomed. Eng. Online* 3:10. **http://www.biomedical-engineering-online.com/content/3/1/10**
41. Guerquin-Kern J-L, Wu T-D, Quintana C, Croisy A. 2005. Progress in analytical imaging of the cell by dynamic secondary ion mass spectrometry (SIMS microscopy). *Biochim. Biophys. Acta* 1724:228–38
42. Guillermier C, Lechene CP, Hill J, Hillion F. 2003. Vacuum bench for the characterization of thermoionization ion sources. *Rev. Sci. Instrum.* 74:3312–16
43. Hancock JF. 2006. Lipid rafts: contentious only from simplistic standpoints. *Nat. Rev. Mol. Cell Biol.* 7:456–62
44. Harbottle RR, Nag K, McIntyre NS, Possmayer F, Petersen NO. 2003. Molecular organization revealed by time-of-flight secondary ion mass spectrometry of a clinically used extracted pulmonary surfactant. *Langmuir* 19:3698–704
45. Hecht B, Sick B, Wild UP, Deckert V, Zenobi R, et al. 2000. Scanning near-field optical microscopy with aperture probes: fundamentals and applications. *J. Chem. Phys.* 112:7761–74
46. Hell SW. 2007. Far-field optical nanoscopy. *Science* 316:1153–58
47. Hell SW, Wichmann J. 1994. Breaking the diffraction resolution limit by stimulated emission. *Opt. Lett.* 19:780–82
48. Hendrickson CL, Emmett MR. 1999. Electrospray ionization Fourier transform ion cyclotron resonance mass spectrometry. *Annu. Rev. Phys. Chem.* 50:517–36
49. Henkel T, Tizard J, Blagburn DJ, Lyon IC. 2007. Interstellar dust laser explorer: a new instrument for elemental and isotopic analysis and imaging of interstellar and interplanetary dust. *Rev. Sc. Instrum.* 78:055107

50. Herrmann AM, Clode PL, Fletcher IR, Nunan N, Stockdale EA, et al. 2007. A novel method for the study of the biophysical interface in soils using nano-scale secondary ion mass spectrometry. *Rapid Commun. Mass Spectrom.* 21:29–34
51. Hillion F, Daigne B, Girard F, Slodzian G. 1993. A new high performance instrument: the CAMECA NanoSIMS 50. In *Secondary Ion Mass Spectrometry: SIMS IX*, ed. A Benninghoven, Y Nihei, R Shimizu, HW Werner, pp. 254–57. New York: Wiley
52. Huang B, Wang W, Bates M, Zhuang X. 2008. Three-dimensional super-resolution imaging by stochastic optical reconstruction microscopy. *Science* 319:810–13
53. Jacoby M. 2006. Bioimaging with mass spectrometry. *Chem. Eng. News* 84:55–56
54. Johansson B. 2006. ToF-SIMS imaging of lipids in cell membranes. *Surf. Interface Anal.* 38:1401–12
55. Klar TA, Jakobs S, Dyba M, Egner A, Hell SW. 2000. Fluorescence microscopy with diffraction resolution limit broken by stimulated emission. *Proc. Nat. Acad. Sci. USA* 97:8206–10
56. Kleinfeld AM, Kampf JP, Lechene C. 2004. Transport of 13C-oleate in adipocytes measured using multi imaging mass spectrometry. *J. Am. Soc. Mass Spectrom.* 15:1572–80
57. Kraft ML, Fishel SF, Galli Marxer C, Weber PK, Hutcheon ID, Boxer SG. 2006. Quantitative analysis of supported membrane composition using the NanoSIMS. *Appl. Surf. Sci.* 252:6950–56
58. Kraft ML, Weber PK, Longo ML, Hutcheon ID, Boxer SG. 2006. Phase-separation of lipid membranes analyzed with high-resolution secondary ion mass spectrometry. *Science* 313:1948–51
59. Lambacher A, Fromherz P. 2002. Luminescence of dye molecules on oxidized silicon and fluorescence interference contrast microscopy of biomembranes. *J. Opt. Soc. Am. B* 19:1435–53
60. Lechene C, Hillion F, McMahon G, Benson D, Kleinfeld AM, et al. 2006. High-resolution quantitative imaging of mammalian and bacterial cells using stable isotope mass spectrometry. *J. Biol.* 5:20.1–20.30. **http://jbiol.com/content/5/6/20**
61. Lechene CP, Luyten Y, McMahon G, Distel DL. 2007. Quantitative imaging of nitrogen fixation within animal cells. *Science* 317:1563–66
62. Legent G, Delaune A, Norris V, Delcorte A, Gibouin D, et al. 2008. Method for macromolecular colocalization using atomic recombination in dynamic SIMS. *J. Phys. Chem. B* 112:5534–46
63. Levi-Setti R. 1988. Structural and microanalytical imaging of biological materials by scanning microscopy with heavy-ion probes. *Annu. Rev. Biophys. Biophys. Chem.* 17:325–47
64. Li L, Cheng J-X. 2008. Label-free coherent anti-stokes Raman scattering imaging of coexisting lipid domains in single bilayers. *J. Phys. Chem. B* 112:1576–79
65. Li T, Wu TD, Mazeas L, Toffin L, Guerquin-Kern JL, et al. 2008. Simultaneous analysis of microbial identity and function using NanoSIMS. *Environ. Microbiol.* 10:580–88
66. Li Z, Verkhoturov SV, Locklear JE, Schweikert EA. 2008. SIMS with C60+ and Au4004+ projectiles: depth and nature of secondary ion emission from multilayer assemblies. *Int. J. Mass Spectrom.* 269:112–117
67. Lin WC, Blanchette CD, Ratto TV, Longo ML. 2006. Lipid asymmetry in DLPC/DSPC-supported lipid bilayers: a combined AFM and fluorescence microscopy study. *Biophys. J.* 90:228–37
68. Liu J, Bartesaghi A, Borgnia MJ, Sapiro G, Subramaniam S. 2008. Molecular architecture of native HIV-1 gp120 trimers. *Nature* 455:109–13
69. Lockyer NP, Vickerman JC. 2004. Progress in cellular analysis using ToF-SIMS. *Appl. Surf. Sci.* 212–232:377–84
70. Mann M, Hendrickson RC, Pandey A. 2001. Analysis of proteins and proteomes by mass spectrometry. *Biochemistry* 70:437–73
71. McDonnell LA, Heeren RMA. 2007. Imaging mass spectrometry. *Mass Spectrom. Rev.* 26:606–43
72. McMahon G, Saint-Cyr HF, Lechene C, Unkefer CJ. 2006. CN-secondary ions form by recombination as demonstrated using multi-isotope mass spectrometry of 13C- and 15N-labeled polyglycine. *J. Am. Soc. Mass Spectrom.* 17:1181–87
73. McQuaw CM, Sostarecz AG, Zheng L, Ewing AG, Winograd N. 2005. Lateral heterogeneity of dipalmitoylphosphatidylethanolamine-cholesterol Langmuir-Blodgett films investigated with imaging mass spectrometry and atomic force microscopy. *Langmuir* 21:807–13
74. McQuaw CM, Zheng L, Ewing AG, Winograd N. 2007. Localization of sphingomyelin in cholesterol domains by imaging mass spectrometry. *Langmuir* 23:5645–50

75. Meibom A, Cuif JP, Houlbreque F, Mostefaoui S, Dauphin Y, et al. 2008. Compositional variations at ultrastructure length scales in coral skeleton. *Geochim. Cosmochim. Acta* 72:1555–69
76. Moerner WE. 2007. New directions in single-molecule imaging and analysis. *Proc. Natl. Acad. Sci. USA* 104:12596–602
77. Moreau JW, Weber PK, Martin MC, Gilbert B, Hutcheon ID, Banfield JF. 2007. Extracellular proteins limit the dispersal of biogenic nanoparticles. *Science* 316:1600–3
78. Musat N, Halm H, Winterholler B, Hoppe P, Peduzzi S, et al. 2008. A single-cell view on the ecophysiology of anaerobic phototrophic bacteria. *Proc. Natl. Acad. Sci. USA* 105:17861–66
79. Oehler DZ, Robert F, Mostefaoui S, Meibom A, Selo M, McKay DS. 2006. Chemical mapping of proterozoic organic matter at submicron spatial resolution. *Astrobiology* 6:838–50
80. Orphan VJ, House CH, Hinrichs K-U, McKeegan KD, DeLong EF. 2001. Methane-consuming Archaea revealed by directly coupled isotopic and phylogenetic analysis. *Science* 293:484–87
81. Ostrowski SG, Szakal C, Kozole J, Roddy TP, Xu J, et al. 2005. Secondary ion MS imaging of lipids in picoliter vials with a buckminsterfullerene ion source. *Anal. Chem.* 77:6190–96
82. Ostrowski SG, Van Bell CT, Winograd N, Ewing AG. 2004. Mass spectrometric imaging of highly curved membranes during *Tetrahymena* mating. *Science* 305:71–73
83. Pachloski ML, Cannon DM, Ewing AG, Winograd N. 1998. Static time-of-flight secondary ion mass spectrometry imaging of freeze-fractured frozen-hydrated biological membranes. *Rapid Commun. Mass Spectrom.* 12:1232–35
84. Pachloski ML, Cannon DM, Ewing AG, Winograd N. 1999. Imaging of exposed headgroups and tail-groups of phospholipid membranes by mass spectrometry. *J. Am. Chem. Soc.* 121:4716–17
85. Parry S, Winograd N. 2005. High-resolution TOF-SIMS imaging of eukaryotic cells preserved in a trehalose matrix. *Anal. Chem.* 77:7950–57
86. Perez JB, Martinez KL, Segura JM, Vogel H. 2006. Supported cell-membrane sheets for functional fluorescence imaging of membrane proteins. *Adv. Funct. Mater.* 16:306–12
87. Popa R, Weber PK, Pett-Ridge J, Finzi JA, Fallon SJ, et al. 2007. Carbon and nitrogen fixation and metabolite exchange in and between individual cells of *Anabaena oscillarioides*. *ISME J.* 1:354–60
88. Prinz C, Malm J, Höök F, Sjovall P. 2007. Structural effects in the analysis of supported lipid bilayers by time-of-flight secondary ion mass spectrometry. *Langmuir* 23:8035–41
89. Quintana C, Bellefqih S, Lawal JY, Guerquin-Kern JL, Wu TD, et al. 2006. Study of the localization of iron, ferritin, and hemosiderin in Alzheimer's disease hippocampus by analytical microscopy at the subcellular level. *J. Struct. Biol.* 153:42–54
90. Quintana C, Wu T-D, Delatour B, Dhenain M, Guerquin-Kern J-L, Croisy A. 2007. Morphological and chemical studies of pathological human and mice brain at the subcellular level: correlation between light, electron, and NanoSIMS microscopies. *Microsc. Res. Tech.* 70:281–95
91. Reyzer ML, Caprioli RM. 2005. MALDI mass spectrometry for direct tissue analysis: a new tool for biomarker discovery. *J. Proteome Res.* 4:1138–42
92. Rickaby REM, Belshaw N, Kilburn M, Taylor A, Grovenor C, Brownlee C. 2004. Submicron-scale coccolith chemistry revealed by NanoSIMS. *Geochim. Cosmochim. Acta* 68:A215
93. Roddy TP, Cannon DM, Meserole CA, Winograd N, Ewing AG. 2002. Imaging of freeze-fractured cells with in situ florescence and time-of-flight secondary ion mass spectrometry. *Anal. Chem.* 74:4011–19
94. Roddy TP, Cannon DM, Ostrowski SG, Winograd N, Ewing AG. 2002. Identification of cellular sections with imaging mass spectrometry following freeze fracture. *Anal. Chem.* 74:4020–26
95. Romer W, Wu TD, Duchambon P, Amessou M, Carrez D, et al. 2006. Sub-cellular localisation of a 15N-labeled peptide vector using NanoSIMS imaging. *Appl. Surf. Sci.* 252:6925–30
96. Sartori A, Gatz R, Beck F, Rigort A, Baumeister W, Plitzko JM. 2007. Correlative microscopy: bridging the gap between fluorescence light microscopy and cryo-electron tomography. *J. Struct. Biol.* 161:135–45
97. Schermelleh L, Carlton PM, Haase S, Sha L, Winoto L, et al. 2008. Subdiffraction multicolor imaging of the nuclear periphery with 3D structured illumination microscopy. *Science* 320:1332–36
98. Shao L, Isaac B, Uzawa S, Agard DA, Sedat JW, Gustafsson MGL. 2008. I5S: wide-field light microscopy with 100-nm-scale resolution in three dimensions. *Biophys. J.* 94:4971–83
99. Sjovall P, Lausmaa J, Johansson B. 2004. Mass spectrometric imaging of lipids in brain tissue. *Anal. Chem.* 76:4271–78

100. Slodzian G, Daigne B, Girard F, Hillion F. 1993. Ion optics for a high resolution scanning ion microscope and spectrometer: transmission evaluations. In *Secondary Ion Mass Spectrometry: SIMS IX*, ed. A Benninghoven, Y Nihei, R Shimizu, HW Werner, pp. 294–97. New York: Wiley
101. Sostarecz AG, Cannon DM Jr, McQuaw CM, Sun S, Ewing AG, Winograd N. 2004. Influence of molecular environment on the analysis of phospholipids by secondary ion mass spectrometry. *Langmuir* 20:4926–32
102. Sostarecz AG, McQuaw CM, Ewing AG, Winograd N. 2004. Phosphatidylethanolamine-induced cholesterol domains chemically identified with mass spectrometric imaging. *J. Am. Chem. Soc.* 126:13882–83
103. Stahlberg H, Walz T. 2008. Molecular electron microscopy: state of the art and current challenges. *ACS Chem. Biol.* 3:268–81
104. Stoeckli M, Chaurand P, Hallahan DE, Caprioli RM. 2001. Imaging mass spectrometry: a new technology for the analysis of protein expression in mammalian tissues. *Nat. Med.* 7:493–96
105. Sykes MT, Williamson JR. 2009. Assembly of the bacterial 30S ribosomal subunit. *Annu. Rev. Biophys.* 38:197–215
106. Touboul D, Halgand F, Brunelle A, Kersting R, Tallarek E, et al. 2004. Tissue molecular ion imaging by gold cluster ion bombardment. *Anal. Chem.* 76:1550–59
107. Touboul D, Roy S, Germain DP, Chaminade P, Brunelle A, Laprevote O. 2007. MALDI-TOF and cluster-TOF-SIMS imaging of Fabry disease biomarkers. *Int. J. Mass Spectrom.* 260:158–65
108. Tyler BJ, Rayal G, Castner DG. 2007. Multivariate analysis strategies for processing ToF-SIMS images of biomaterials. *Biomaterials* 28:2412–23
109. Usami N, Furusawa Y, Kobayashi K, Lacombe S, Reynaud-Angelin A, et al. 2008. Mammalian cells loaded with platinum-containing molecules are sensitized to fast atomic ions. *Int. J. Rad. Biol.* 84:603–11
110. Verhaeghe E, Fraysse A, Guerquin-Kern J-L, Wu T-D, Devès G, et al. 2007. Microchemical imaging of iodine distribution in the brown alga *Laminaria digitata* suggests a new mechanism for its accumulation. *J. Biol. Inorg. Chem.* 13:257–69
111. Wang H, Obenauer-Kutner L, Lin M, Huang Y, Grace MJ, Lindsay SM. 2008. Imaging glycosylation. *J. Am. Chem. Soc.* 130:8154–55
112. Westphal V, Rizzoli SO, Lauterbach MA, Kamin D, Jahn R, Hell SW. 2008. Video-rate far-field optical nanoscopy dissects synaptic vesicle movement. *Science* 320:246–49
113. Wilson RG, Stevie FA, Magee CW. 1989. *Secondary Ion Mass Spectrometry: A Practical Handbook for Depth Profiling and Bulk Impurity Analysis*. New York: Wiley
114. Wiseman JM, Ifa DR, Zhu Y, Kissinger CB, Manicke NE, et al. 2008. Desorption electrospray ionization mass spectrometry: imaging drugs and metabolites in tissues. *Proc. Natl. Acad. Sci. USA* 105:18120–25
115. Wittig A, Arlinghaus HF, Kriegeskotte C, Moss RL, Appelman K, et al. 2008. Laser postionization secondary neutral mass spectrometry in tissue: A powerful tool for elemental and molecular imaging in the development of targeted drugs. *Mol. Cancer Ther.* 7:1763–71
116. Yu ML. 1982. Matrix effects in the work-function dependence of negative-secondary-ion emission. *Phys. Rev. B* 26:4731–34
117. Zheng H, Chu J, Qiu Y, Loh HH, Law P. 2008. Agonist-selective signaling is determined by the receptor location within the domains. *Proc. Natl. Acad. Sci. USA* 105:9421–26
118. Zumholz K, Hansteen T, Hillion F, Horreard F, Piatkowski U. 2007. Elemental distribution in cephalopod statoliths: NanoSIMS provides new insights into nano-scale structure. *Rev. Fish Biol. Fish.* 17:487–91

Annual Review of Biophysics
Volume 38, 2009

Contents

Index

Errata

An online log of corrections to *Annual Review of Biophysics* articles may be found at http://biophys.annualreviews.org/errata.shtml